Kinetics and Mechanism of Iron(III) Dissociation from the Dihydroxamate Siderophores Alcaligin and Rhodotorulic Acid

Hakim Boukhalfa,[†] Timothy J. Brickman,[‡] Sandra K. Armstrong,[‡] and Alvin L. Crumbliss*,[†]

Department of Chemistry, Duke University, Box 90346, Durham, North Carolina 27708-0346, and Department of Microbiology, University of Minnesota, Minneapolis, Minnesota 55455-0312

Received March 28, 2000

The kinetics and mechanism of siderophore ligand dissociation from their fully chelated Fe(III) complexes is described for the highly preorganized cyclic tetradentate alcaligin and random linear tetradentate rhodotorulic acid in aqueous solution at 25 °C ($Fe_2L_3 + 6H^+ \rightleftharpoons 2\ Fe^{3+}_{aq} + 3\ H_2L$). At siderophore:Fe(III) ratios where Fe(III) is hexacoordinated, kinetic data for the H^+-driven ligand dissociation from the Fe_2L_3 species is consistent with a singly ligand bridged structure for both the alcaligin and rhodotorulic acid complexes. Proton-driven ligand dissociation is found to proceed via parallel reaction paths for rhodotorulic acid, in contrast with the single path previously observed for the linear trihydroxamate siderophore ferrioxamine B. Parallel paths are also available for ligand dissociation from $Fe_2(alcaligin)_3$, although the efficiency of one path is greatly diminished and dissociation of the bis coordinated complex $Fe(alcaligin)(OH_2)_2^+$ is extremely slow ($k = 10^{-5}\ M^{-1}\ s^{-1}$) due to the high degree of preorganization in the alcaligin siderophore. Mechanistic interpretations were further confirmed by investigating the kinetics of ligand dissociation from the ternary complexes Fe(alcaligin)(L) in aqueous acid where L = *N*-methylacetohydroxamic acid and glycine hydroxamic acid. The existence of multiple ligand dissociation paths is discussed in the context of siderophore mediated microbial iron transport.

Introduction

Siderophores are a class of microbially synthesized compounds for the purpose of solubilizing environmental iron and making this essential element bioavailable to the cell. The hydroxamate moiety is the most common Fe(III) specific binding unit found in siderophores produced by fungi, molds, and yeast.[1−5] Siderophores are most commonly hexadentate ligands in order to completely sequester Fe(III) and bring it to the cell without hydrolysis or ligand dissociation occurring.[2] However, tetradentate dihydroxamic acid bacterial siderophore structures are known, such as the linear rhodotorulic acid (H_2L^{RA})[6−10] from *Rhodotorula pilimanae* and the cyclic alcaligin (H_2L^{AG})[11−14] produced by the heterotrophic bacterium *Alcaligenes denitrificans* KN3-J and *Alcaligenes xylosoxidans*, and the human respiratory pathogens *Bordetella pertussis* and *Bordetella bronchiseptica*. Since in these cases a single siderophore molecule cannot satisfy the six coordination sites for Fe(III), the dihydroxamate siderophores form bimetallic complexes of stoichiometry Fe_2L_3 in order to coordinatively saturate the iron.[6−9,15,16] Thermodynamic investigations of Fe(III) complexes of rhodotorulic acid[6,7] and alcaligin[15] characterized the equilibrium involved in the formation of fully coordinated iron complexes as illustrated in eqs 1 and 2 (coordinated water omitted for clarity). The X-ray crystal structure of the diiron

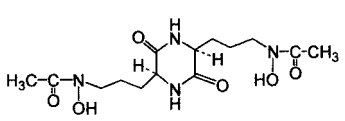

Rhodotorulic acid (H_2L^{RA})

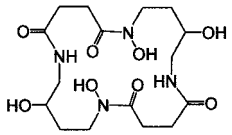

Alcaligin (H_2L^{AG})

$$Fe^{3+} + H_2L \rightleftharpoons Fe(L)^+ + 2H^+ \quad (1)$$

$$2Fe(L)^+ + H_2L \rightleftharpoons Fe_2(L)_3 + 2H^+ \quad (2)$$

complex of alcaligin shows a bimetallic singly-ligand-bridged structure where the two metal centers are separated through a

* Address correspondence to this author: alc@chem.duke.edu. Fax: (919) 660-1605.
[†] Duke University.
[‡] University of Minnesota.

(1) Raymond, K. N.; Telford, J. R. In *Bioinorganic Chemistry: An Inoganic Perspective of Life*; Kessissoglou, D. P., Ed.; NATO ASI Series C: Mathematical and physical Science, Vol. 459; Kluwer Academic Publishers: Dordrecht, The Netherlands, 1995; p 25.
(2) Albrecht-Gary, A.-M.; Crumbliss, A. L. In *Iron Transport and Storage in Microoganisms, Plants and Animals*, Vol. 35 of *Metal Ions in Biological Systems*; Sigel, A., Sigel, H., Eds.; M. Dekker, Inc.: New York, 1998; p 239.
(3) Albrecht-Gary, A.-M.; Crumbliss, A. L. In *Scientific bridges for 2000 and Beyond*; Institut de France, Académie des Science, Editions TEC & DOC, Paris: 1999; p 73.
(4) Winkelmann, G., Carrano, C. J., Eds. *Transition Metals in Microbial Metabolism*; Harwood Academic Publishers: U.K., 1997.
(5) Telford, J. R.; Raymond, K. N. In *Molecular Recognition: Receptors for Cationic Guests*, Vol. 1 of *Comprehensive Supramolecular Chemistry*; Lehn, J.-M., Exec. Ed.; Gokel, G. W., Vol. Ed.; Pergamon Press: London, 1996; p 245.
(6) Carrano, C. J.; Cooper, S. R.; Raymond, K. N. *J. Am. Chem. Soc.* **1979**, *101*, 599.
(7) Carrano, C. J.; Raymond, K. N. *J. Bacteriol.* **1978**, *136*, 69.
(8) Müller, G.; Isowa, Y.; Raymond, K. N. *J. Biol. Chem.* **1985**, *260*, 13921.
(9) Müller, G.; Barclay, S. J.; Raymond, K. N. *J. Biol. Chem.* **1985**, *260*, 13916.
(10) Atkin, C. L.; Neilands, J. B. *Biochemistry* **1968**, *7*, 3734.
(11) Nishio, T.; Ishida, Y. *Agric. Biol. Chem.* **1990**, *54*, 1837.
(12) Nishio, T.; Tanaka, N.; Hiratake, J.; Katsube, Y.; Ishida, Y.; Oda, J. *J. Am. Chem. Soc.* **1988**, *110*, 8733.
(13) Brickman, T. J.; Hansel, J. G.; Miller, M. J.; Armstrong, S. K. *BioMetals* **1996**, *9*, 191.

10.1021/ic000330k CCC: $19.00
Published on Web 11/21/2000

rigid carbon chain in which the two metal centers are noninteracting.[16] Comparison of the Fe(III)-complex crystal structure with that of metal-free alcaligin[12] demonstrates that the terminally bound alcaligin ligand exhibits a high degree of preorganization. This observation was confirmed by solution thermodynamic studies that showed an enhanced stability constant for reaction 1.[15−17]

Structural investigations of the solution equilibria associated with alcaligin and rhodotorulic acid chelation of Fe(III) by electrospray ionization mass spectrometry (ESI-MS) have also been reported,[18] and two major tris hydroxamate coordinated species were identified at neutral pH. In addition to the bimetallic species $Fe_2(L^{AG})_3$, a mono-Fe complex of the structure $Fe(L^{AG})(HL^{AG})$ was also observed.[18] The structure of the rhodotorulic acid complex $Fe_2(L^{RA})_3$ has been interpreted as a di-Fe triply bridged complex. This assignment is supported by the X-ray crystal structure of a synthetic analogue which exhibits a triply bridged coordination mode.[19] From our recent ESI-MS investigation at an $Fe:H_2L^{RA}$ ratio of 2:3, the major hexacoordinated tris complex in aqueous solution is a mono-Fe species of stoichiometry $Fe(L^{RA})(HL^{RA})$.[18]

The dissociation kinetics and reaction mechanism of the hexadentate trihydroxamate siderophore ferrioxamine B have been investigated.[20,21] The results of these studies demonstrate an extreme kinetic and thermodynamic stability for the iron complex afforded by complete coordination of the Fe(III) center. The dihydroxamic acid siderophores alcaligin and rhodotorulic acid form mono- and bimetallic multidentate complexes. A comparative kinetic investigation of alcaligin and rhodotorulic acid complexes of Fe(III) is important for probing the relationship between metal complex structure and ligand exchange mechanism relevant to biological iron transport. For example, although both alcaligin and rhodotorulic acid produce Fe(III) complexes with the common stoichiometry Fe_2L_3, there are significant structural differences which make a comparative kinetics study particularly interesting. These include the singly bridged and assumed triply bridged structures for $Fe_2(L^{AG})_3$ and $Fe_2(L^{RA})_3$, respectively, and a high degree of preorganization for cyclic alcaligin[15,16] and no preorganization for the linear rhodotorulic acid.

As part of our ongoing investigations of Fe(III) complexes of dihydroxamate siderophores and siderophore models,[18,22−28] we report here the kinetics and mechanism of Fe(III) release from its alcaligin and rhodotorulic acid complexes. Of particular interest is the elucidation of additional reactive pathways afforded by the tetradentate dihydroxamate structure relative to the hexadentate siderophore complexes, as was illustrated in our recent report on the kinetics of Fe(III) release from synthetic dihydroxamic acid complexes.[22] Since the biological function of a siderophore includes the critical event of releasing the Fe at the cell, the kinetics and mechanism of Fe(III) release from alcaligin and rhodotorulic acid complexes are of additional significance.

Experimental Section

Materials. Complex and acid solutions were prepared in deionized water, and the pH measurements were made using a Corning 250 pH/ion meter equipped with an Orion ROSS pH electrode filled with 3.0 M NaCl solution. pH adjustment was made by dropwise addition of 0.1 M NaOH or 0.1 M $HClO_4$ to obtain the desired acidity. Stock solutions of 2.0 M $NaClO_4$ were prepared from solid sodium perchlorate hydrate (Aldrich 99+%) and standardized by passing through a Dowex 50 W-X8 strong acid cation-exchange column in H^+ form. The 2.0 M $HClO_4$ stock solution was prepared from concentrated perchloric acid (Fisher 70%) and standardized by titration with standard NaOH solution to the phenolphthalein end point. Ferric perchlorate stock solution (0.1 M) was prepared from recrystallized ferric perchlorate hydrate and standardized spectrophotometrically in strong acid[29] and titrimetrically by reduction with Sn(II) and titrating with the primary standard potassium dichromate.[30]

Ligand and Fe(III) Complex Preparation. Rhodotorulic acid (H_2L^{RA}) was purchased from Aldrich. Alcaligin (H_2L^{AG}) was prepared and characterized as described elsewhere.[31] Purity for both siderophores was established by mass spectrometry and UV−visible spectra of the Fe(III) complex. *N*-Methylacetohydroxamic acid (NMAHA) was synthesized as described in the literature.[32] The tris(hydroxamato)iron(III) complexes of alcaligin $Fe_2(L^{AG})_3$ and $Fe_2(L^{RA})_3$ were prepared by reacting $Fe(ClO_4)_3$ with the dihydroxamate ligands H_2L^{AG} and H_2L^{RA} in a 2:3 Fe(III)-to-ligand ratio, and the pH was adjusted to neutral (pH = 6.5−7.5) by adding NaOH or $HClO_4$ and the ionic strength maintained at $I = 2.0$ by $NaClO_4$. All tris complexes were characterized by comparing their UV−visible spectra to literature results (λ_{max} at 425 nm, $\epsilon = 2600-2800$ M^{-1} cm^{-1} per Fe).[6,20,21,25] Ternary complexes of alcaligin and *N*-methylacetohydroxamic acid (NMAHA) were prepared by adding 1 equiv of the monohydroxamic acid ligand to a solution of the alcaligin−Fe(III) complex, $Fe(L^{AG})^+$, formed by reacting the alcaligin ligand in a 1:1 Fe:L ratio with an equivalent amount of 0.1 M $Fe(ClO_4)_3$. The tris(hydroxamato)iron(III) complexes were formed in neutral pH; the complex solution shows a strong absorbance at $\lambda_{max} = 425$ nm ($\epsilon = 2600-2800$ M^{-1} cm^{-1} per Fe).

Kinetic Measurements. Kinetic measurements were performed by rapid mixing of an aqueous solution of the Fe(III) complex with an aqueous solution at the desired proton concentration ($HClO_4$) using an Applied Photophysics stopped-flow instrument (SX.18 MV), equipped with a diode array spectrophotometer with an approximate range of 200−750 nm. Both solutions were maintained at $I = 2.0$ M ($NaClO_4$/$HClO_4$) and thermostated at 25 °C. The absorbance decay due to ligand dissociation was followed at 425 nm at various proton concentrations (0.0001−1.0 M). All measurements were performed under pseudo-first-order conditions of excess acid at 25 °C and constant ionic strength $I = 2.0$ M ($NaClO_4$/$HClO_4$). The signals of the absorbance change were

(14) Moore, C. H.; Foster, L. A.; Gerbig, D. G.; Dyer, D. W., Jr.; Gibson, B. W. *J. Bacteriol*. **1995**, *177*, 1116.
(15) Hou, Z.; Raymond, K. N.; O'Sullivan, B.; Esker, T. W.; Nishio, T. *Inorg. Chem*. **1998**, *37*, 6630.
(16) Hou, Z.; Sunderland, C. J.; Nishio, T.; Raymond, K. N. *J. Am. Chem. Soc*. **1996,** *118*, 5148.
(17) Crumbliss, A. L. *ChemTracts* **1997**, *10*, 354.
(18) Spasojevic′, I.; Boukhalfa, H.; Stevens, R. D.; Crumbliss, A. L. *Inorg. Chem.*, in press.
(19) Scarrow, R. C.; White, D. L.; Raymond, K. N. *J. Am. Chem. Soc*. **1985**, *107*, 6540.
(20) Monzyk, B.; Crumbliss, A. L. *J. Am. Chem. Soc.* **1982**, *104*, 4921.
(21) Biruš, M.; Bradic, Z.; Krzanric, G.; Kijundzic, N.; Pribanic, M.; Wilkins, P. C.; Wilkins, R. G. *Inorg. Chem*. **1987**, *26*, 1000.
(22) Boukhalfa, H.; Crumbliss, A. L. *Inorg. Chem.* **2000**, *39*, 4318.
(23) (a) Chaubet, F.; Nguyen Van Duong, M.; Gref, A.; Courtieu, J.; Crumbliss, A. L.; Gaudemer, A. *Tetrahedron Lett*. **1990**, *31*, 5729. (b) Chaubet, F.; Nguyen Van Duong, K.; Courtieu, J.; Gaudemer, A.; Gref, A.; Crumbliss, A. L. *Can. J. Chem*. **1991**, *69*, 1107. (c) Chaubet F.; Nguyen Van Duong, K.; Courtieu, J.; Gaudemer, A.; Gref, A.; Crumbliss A. L.; Caudle, M. T. *Can. J. Chem.* **1994**, *72*, 2361.
(24) Spasojevic′, I.; Armstrong, S. K.; Brickman, T. J.; Crumbliss, A. L. *Inorg. Chem*. **1999**, *38*, 449.
(25) Caudle, M. T.; Cogswell, L. P., III; Crumbliss, A. L. *Inorg. Chem*. **1994**, *33*, 4759.
(26) Caudle, M. T.; Crumbliss, A. L. *Inorg. Chem*. **1994**, *33*, 4077.
(27) (a) Monzyk, B.; Crumbliss, A. L. *J. Am. Chem. Soc*. **1979**, *101*, 6203. (b) Brink C. P.; Crumbliss, A. L. *Inorg. Chem*. **1984**, *23*, 4708
(28) (a) Caudle, M. T.; Stevens, R. D.; Crumbliss, A. L. *Inorg. Chem*. **1994**, *33*, 843. (b) Caudle, M. T.; Stevens, R. D.; Crumbliss, A. L. *Inorg. Chem*. **1994**, *33*, 6111.
(29) Bastian, R.; Weberling, R.; Palilla, F. *Anal. Chem*. **1956**, *28*, 459.
(30) Vogel. A. I. *Quantitative Inorganic Analysis Including Elementary Instrumental Analysis*, 3rd ed.; Longmans, Green and Co., Ltd.: London, 1968.
(31) Brickman, T. J.; Hansel, J. G.; Miller, M. J.; Armstrong, S. K. *BioMetals* **1996**, *9*, 191.
(32) Hauser, C. R.; Renfrow, W. B. *Org. Synth*. **1943**, *2*, 67.

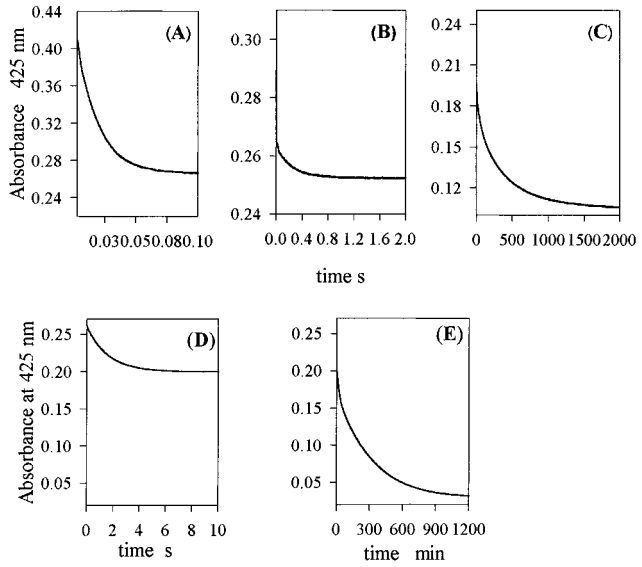

Figure 1. Absorbance decay at 425 nm recorded with time during the H^+-driven dissociation of rhodotorulic acid−iron(III) and alcaligin−iron(III) complexes prepared at neutral pH, $I = 2$ M ($HClO_4/NaClO_4$), $T = 25$ °C. Panels A−C: $[Fe^{3+}] = 0.15$ mM, $[H_2L^{RA}] = 0.23$ mM, $\lambda = 425$ nm (optical path 1 cm), $[H^+] = 0.004$ M (A), 0.1 M (B), 0.55 M (C). Panels D and E: $[Fe^{3+}] = 0.1$ mM, $[H_2L^{AG}] = 0.15$ mM, $\lambda = 425$ nm (optical path 1 cm), $[H^+] = 0.004$ M (D) and 0.55 M (E).

fitted according to the appropriate model using the Applied Photophysics kinetic software.

Results

General Observations. Dihydroxamic acid siderophores form Fe(III) complexes of different stoichiometry depending on the pH range and the metal-to-ligand ratio.[6,15,18,28] The observed λ_{max} is sensitive to the formation of bis hydroxamate ($\lambda_{max} = 470$ nm; $\epsilon = 1500-1800$ cm^{-1} M^{-1} per Fe) and tris hydroxamate ($\lambda_{max} = 425-430$ nm; $\epsilon = 2500-2800$ cm^{-1} M^{-1} per Fe) coordination to Fe(III), with an isosbestic point for interconversion between the two coordination modes at 470 nm.[6,15,22] Tris hydroxamato Fe(III) complexes are stable at neutral pH, and, as the pH is lowered to more acidic media (pH = 2), the tris complex dissociates to the bis complex.

The tris Fe(III) complex of alcaligin is prepared by mixing the appropriate amount of the ligand and Fe^{3+}_{aq} solution in a 2:3 Fe:L^{AG} ratio. The solution turns a red-orange color characteristic of the tris complex after the pH is increased to 6.5−7, and the UV−visible spectra exhibit an absorbance band at $\lambda_{max} = 425$ nm. The dissociation kinetics of the tris alcaligin−Fe(III) complex were studied in the H^+ concentration range from 0.001 to 0.07 M. The spectral changes recorded during H^+-driven ligand dissociation exhibit isosbestic behavior characteristic of tris to bis hydroxamato Fe(III) complex conversion. The Fe(III) complex of rhodotorulic acid prepared in the same way shows similar behavior with slight differences.

The absorbance decay at 425 nm recorded during the H^+-driven ligand dissociation show multistep behavior for both siderophore complexes. For rhodotorulic acid, a fast drop of the initial absorbance is followed by a double-exponential absorbance decay, a relatively slow mono-exponential decay, and finally a slow monoexponential decay is observed (Figure 1, plots A, B, and C). For alcaligin, a monoexponential absorbance decay is followed by a double-exponential absorbance change, as shown in Figure 1, plots D and E. Reaction schemes describing the dissociation kinetics of rhodotorulic acid and alcaligin complexes with Fe(III) will be presented individually.

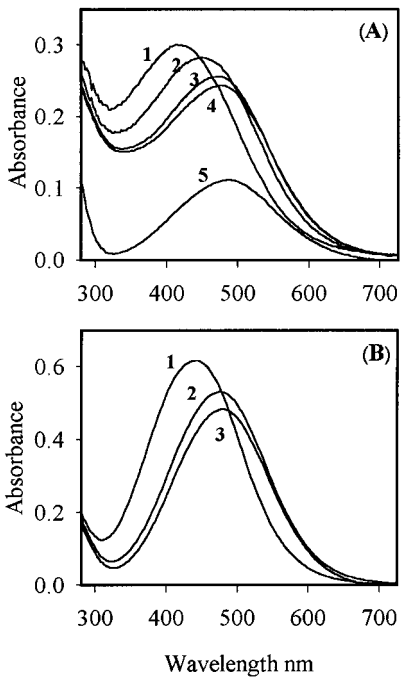

Figure 2. UV−visible spectra collected at different stages of the H^+-driven dissociation of rhodotorulic acid−iron(III) and alcaligin−iron(III) complexes. A: $[Fe^{3+}] = 0.13$ mM, $[H_2L^{RA}] = 0.20$ mM, $I = 2.0$ M ($HClO_4/NaClO_4$), $T = 25$ °C. (A) (1) Spectrum of the starting complex at pH = 7.5; (A) (2) spectrum recorded within 5 ms after mixing with 0.004 M $HClO_4$; (A) (3 and 4) spectra recorded 350 ms and 2 s after mixing with 0.004 M $HClO_4$ solution; (A) (5) spectrum collected after 2000 s at $[H^+] = 0.55$ M. (B) $[Fe^{3+}] = 0.2$ mM, $[H_2L^{AG}] = 0.3$ mM, $I = 2.0$ M ($HClO_4/NaClO_4$), $T = 25$ °C. (B) (1) spectrum of the starting complex at pH = 6.65; (B) (2) spectrum collected at the end of the first absorbance decay at $[H^+] = 0.01$ M; (B) (3) spectrum collected at $[H^+] = 0.4$ M after 2500 s.

Ligand Dissociation Kinetics for the Rhodotorulic Acid−Iron(III) Complex. (A) Ligand Dissociation Kinetics of the Tris Complex. The tris hydroxamate−Fe(III) complex formed with rhodotorulic acid was prepared in a 2:3 Fe:L^{RA} ratio. Ligand dissociation from the tris complex was monitored at 425 nm by rapid mixing of the complex prepared at neutral pH (0.2 mM of the complex) with an equal volume of $HClO_4$ of the desired concentration ($[H^+] = 0.001-0.012$ M, $T = 25$ °C and $I = 2.0$ M ($NaClO_4/HClO_4$)). The absorbance change recorded under these conditions gave a rapid absorbance decrease within a few milliseconds, followed by a double-exponential absorbance decay (Figure 1A), followed by a monoexponential decay (Figure 1B). Time dependent spectra recorded during this H^+-driven ligand dissociation reaction are shown in Figure 2A. The fast absorbance drop produces a significant shift in the absorbance maximum to longer wavelength, $\lambda_{max} = 460$ nm (spectra 1 and 2); the second and third steps show isosbestic behavior (spectra 2−4). The isosbestic point associated with the first set of these spectra is situated at 495 nm, and the absorbance maximum is at 470 nm. The second set of spectra has an isosbestic point at 584 nm, and the absorbance maximum is shifted above 470 nm (Figure 2A). In excess ligand (Fe^{3+}:L^{RA} ratio 2:4) the dissociation from tris to bis complex shows a monoexponential absorbance decay. The corresponding time dependent spectra show an isosbestic point at 470 nm (data not shown).

The ligand dissociation process associated with the first very fast step (reactions 4 and 4′) was too fast to obtain accurate kinetic data. Evidence for the very fast step comes from comparing the initial spectrum ($\lambda_{max} = 425$ nm) to the spectra

recorded after mixing with the acid solution (λ_{max} = 460 nm; Figure 2A, spectra 1 and 2). The apparent dissociation rate constants for the second and third steps were obtained by fitting the second absorbance decay as a double-exponential signal as shown in eq 3.

$$A - A_{eq} = Be^{-k_{10}t} + Ce^{-k'_{10}t} \quad (3)$$

The two apparent dissociation rate constants determined in this way show linear behavior with $[H^+]$ (Figure 3A). The kinetic data for the overall dissociation of the tris complex is interpreted in terms of reactions 4−6 in Scheme 1.

Scheme 1

$$Fe(L^{RA})(HL^{RA}) + H^+ \rightleftharpoons Fe(HL^{RA})_2^{+*} \qquad K_{11} \quad (4)$$

$$Fe(L^{RA})(HL^{RA}) + H^+ \rightleftharpoons Fe(L^{RA})(H_2L^{RA})^{+**} \qquad K'_{11} \quad (4')$$

$$Fe(HL^{RA})_2^{+*} \rightleftharpoons Fe(HL^{RA})_2^{+} \qquad k_{10}, k_{-10} \quad (5)$$

$$Fe(L^{RA})(H_2L^{RA})^{+**} \rightleftharpoons Fe(L^{RA})^{+} + H_2L^{RA} \qquad k'_{10}, k'_{-10} \quad (6)$$

Scheme 1 is composed of two parallel competitive pathways, reactions 4 and 5, and 4′ and 6, in which the tris complex Fe(L^{RA})(HL^{RA}) reacts with H^+ at two different sites to form two different bis complex species, Fe(HL^{RA})$_2^+$ and Fe(L^{RA})$^+$, as illustrated in Scheme 2. The complex Fe(L^{RA})(HL^{RA}) has three coordinated hydroxamate units.

Scheme 2

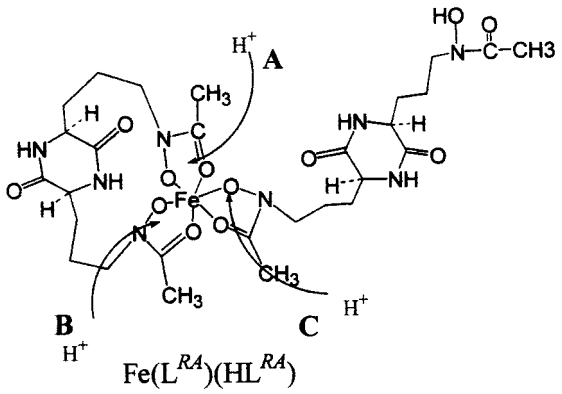

The first protonation can occur equally at each site (A, B, and C in Scheme 2) leading to two different intermediates Fe(HL^{RA})$_2^{+*}$ and Fe(L^{RA})(H_2L^{RA})$^{+**}$, which may exhibit slightly different spectra. The dissociation proceeds in two steps, a rapid protonation pre-equilibrium, eqs 4 and 4′, followed by a proton independent reaction in eqs 5 and 6. The fast absorbance decay is attributed to the rapid pre-equilibrium (eqs 4 and 4′), and the double-exponential decay is attributed to the dissociation of the two intermediates Fe(HL^{RA})$_2^{+*}$ and Fe(L^{RA})(H_2L^{RA})$^{+**}$ according to reactions 5 and 6.

The rate law associated with the reaction in Scheme 1 is expressed for the conditions where $[H^+] \gg [Fe(L^{RA})(HL^{RA})]$ according to eqs 7a and 7b, by assuming that reactions 4 and 4′

$$k_{10}^{obsd} = \frac{k_{10}K_{11}[H^+]}{1 + K_{11}[H^+] + K'_{11}[H^+]} + k_{-10} \quad (7a)$$

$$k'^{obsd}_{10} = \frac{k'_{10}K'_{11}[H^+]}{1 + K_{11}[H^+] + K'_{11}[H^+]} + k'_{-10} \quad (7b)$$

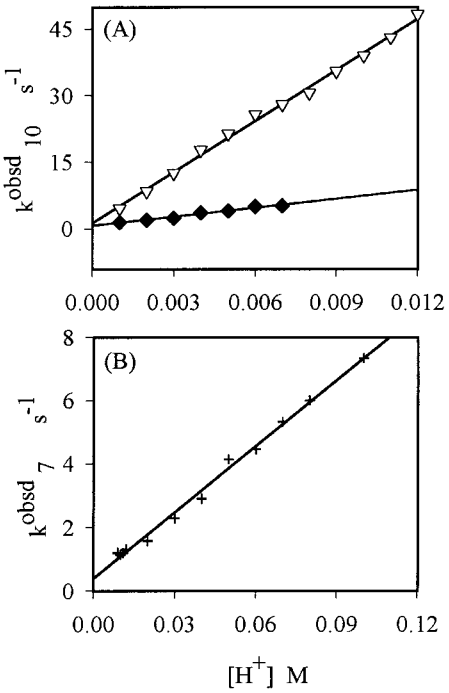

Figure 3. Plot of the observed dissociation rate constants k_{10}^{obsd}, k'^{obsd}_{10}, and k_7^{obsd} for the dissociation of Fe(L^{RA})(HL^{RA}) as a function of $[H^+]$. A: (▽) k_{10}^{obsd} and (◆) k'^{obsd}_{10} were obtained from analyzing the absorbance decay signal on a 0.1 s time scale (Figure 1A) as a double-exponential decay (eq 3). B: (+) k_7^{obsd} obtained by analyzing the third absorbance decay (Figure 1B) as a monoexponential. Conditions: I = 2.0 M ($HClO_4$/$NaClO_4$), $[Fe^{3+}]$ = 0.15 mM, $[H_2L^{RA}]$ = 0.23 mM, T = 25 °C. Solid lines represent fits of linear equations to the data: (A) (▽) $k_{10}^{obsd} = a[H^+] + b$; see eq 8a. $a = 3.84 \times 10^3$ (76), b = 1.4(0.5). (A) (◆) $k'^{obsd}_{10} = a[H^+] + b$; see eq 8b. a = 678 (36), b = 0.7(0.2). (B) (+) $k_7^{obsd} = a[H^+] + b$; see eq 10. a = 69 (2), b = 0.3 (0.1).

are rapid pre-equilibria established before reactions 5 and 6 proceed. This assumption is supported by the very fast absorbance decrease that occurs in a few milliseconds after mixing. The apparent dissociation rate constants k_{10}^{obsd} and k'^{obsd}_{10} at low proton concentration are proportional to $[H^+]$; however, at higher H^+ they may become $[H^+]$ independent. In the $[H^+]$ range investigated (0.001−0.07 M) the apparent dissociation constant shows linear behavior with respect to $[H^+]$, suggesting a simple rate law as in eqs 8a and 8b. The values of $K_{11}k_{10}$ and $K'_{11}k'_{10}$

$$k_{10}^{obsd} = k_{10}K_{11}[H^+] + k_{-10} \quad (8a)$$

$$k'^{obsd}_{10} = k'_{10}K'_{11}[H^+] + k'_{-10} \quad (8b)$$

determined by a linear fit of eqs 8a and 8b to the experimental data (Figure 3A) are $K_{11}k_{10}$ = 678 M^{-1} s^{-1} and $K'_{11}k'_{10}$ = 3839 M^{-1} s^{-1}.

The third absorbance decay is associated with the dissociation of the intermediate Fe(HL^{RA})$_2^+$ through reaction 9. The rate law

$$Fe(HL^{RA})_2^+ + H^+ \rightleftharpoons Fe(HL^{RA})^{2+} + H_2L^{RA} \qquad k_7, k_{-7} \quad (9)$$

associated with reaction 9 is expressed according to experimental data by eq 10. The dissociation rate constant k_7 was determined from a linear fit of eq 10 to the experimental data (Figure 3B);

$$k_7^{obsd} = k_7[H^+] + k_{-7}[H_2L^{RA}] \quad (10)$$

k_7 = 69 M^{-1} s^{-1}. The value of k_7 is in good agreement with dissociation rate constants observed for synthetic dihydroxamate

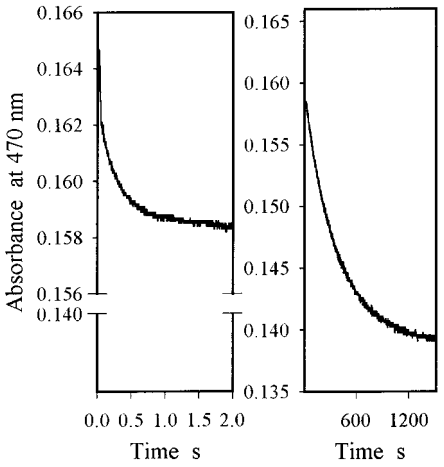

Figure 4. Absorbance decay at $\lambda = 470$ nm (optical path 1 cm) recorded with time during the acid dissociation of $Fe(L^{RA})^+$ prepared in a 1:1 Fe:L^{RA} ratio. Conditions: $[Fe^{3+}] = 0.1$ mM, $[H_2L^{RA}] = 0.1$ mM, $[H^+] = 0.25$ M, $I = 2.0$ M ($HClO_4/NaClO_4$), $T = 25$ °C.

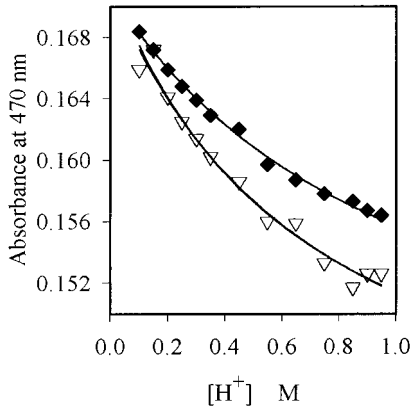

Figure 5. Plot of the absorbance at a quasi equilibrium position as a function of $[H^+]$ for the dissociation of the bis Fe(III)−rhodotorulic acid complex. Data collected at 470 nm after the fast absorbance drop (◆) and at the end of the first absorbance decay observed (▽). Complex prepared in a 1:1 Fe:L ratio: $[Fe^{3+}] = 0.2$ mM, $[H_2L^{RA}] = 0.2$ mM, pH = 2.0, $I = 2.0$ M ($HClO_4/NaClO_4$), $T = 25$ °C. The solid lines represent fits of eqs 15 (◆) and 16 (▽) to the data. The convergence parameters are as follows: (◆) $\epsilon_{Fe(L^{RA})^+} = 1717$ (46), $\epsilon_{Fe(HL^{RA})^{2+*}} = 1440$ (17) M^{-1} cm^{-1}, $K_5 = 1.31$ (0.2). (▽) $\epsilon_{Fe(HL^{RA})^{2+*}} = 1394$ (419), and $\epsilon_{Fe(HL^{RA})^{2+}} = 1162$ (275) M^{-1} cm^{-1}. The values for K_5 and $\epsilon_{Fe(L^{RA})^+}$ were fixed at $K_5 = 1.31$ and $\epsilon_{Fe(L^{RA})^+} = 1717$ M^{-1} cm^{-1}. Values in parentheses represent the standard error.

complexes of the same structure $(Fe(HL^n)_2^+)$.[22] The species $Fe(HL^{RA})_2^+$ is a transient intermediate produced during the H^+-driven dissociation of the tris complex and is not present in solution as a stable species. The transient existence of this species is consistent with our ESI-MS study in which we found no evidence for $Fe(HL^{RA})_2^+$.[18]

(B) Ligand Dissociation Kinetics of the Bis Complex Fe-(L^{RA})$^+$. The complex prepared in a 1:1 Fe:L^{RA} ratio at pH 2 shows a strong absorbance at 470 nm, characteristic of a bis hydroxamate Fe(III) complex. Rapid mixing of the complex solution with $HClO_4$ ($[H^+] = 0.1-1.0$ M) results in a multistep ligand dissociation process. The absorbance change recorded during the H^+-driven ligand dissociation shows a very fast absorbance drop, followed by a double-exponential absorbance decay (Figure 4). The amplitude of the very fast absorbance drop is $[H^+]$ dependent. The reaction involved in the very fast step is too fast to be monitored by stopped-flow spectrophotometry. However, the amplitude of the absorbance drop with respect to $[H^+]$ was used to define the number of protons involved and to define the dissociation equilibrium constant associated with this process. This very fast reaction is followed by two successive absorbance decays monitored in the time ranges of 2 s and 1500 s (Figure 4). The ligand dissociation process results in a shift of λ_{max} to longer wavelength (Figure 2A; spectra 4 and 5). This result is interpreted in terms of successive dissociation reactions, as illustrated in Scheme 3.

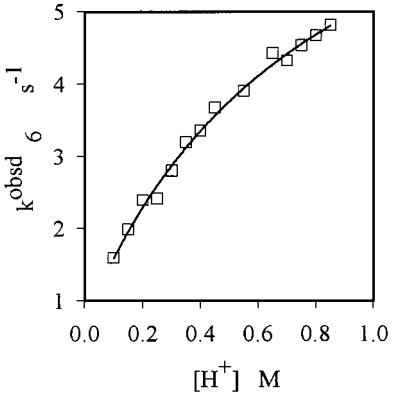

Figure 6. Variation of the observed dissociation rate constant k_6^{obsd} as a function of $[H^+]$ for $Fe(L^{RA})^+$ prepared in a 1:1 Fe:L^{RA} ratio. Conditions: $[Fe^{3+}] = 0.1$ mM, $[L^{RA}] = 0.1$ mM, $I = 2.0$ M ($HClO_4/NaClO_4$), $T = 25$ °C, $[H^+] = 0.1-1.0$ M. The solid line represents the fit of eq 17 to the experimental data with convergence parameters $k_6 = 7.98$ (0.65) s^{-1}, $K_5 = 1.25$ (0.28) M^{-1}, $k_{-6} = 0.7$ (0.2) s^{-1}. Values in parentheses represent the standard error.

Scheme 3

$$Fe(L^{RA})^+ + H^+ \rightleftharpoons Fe(HL^{RA})^{2+*} \qquad K_5 \qquad (11)$$

$$Fe(HL^{RA})^{2+*} \rightleftharpoons Fe(HL^{RA})^{2+} \qquad k_6, k_{-6}, K_6 \qquad (12)$$

$$Fe(HL^{RA})^{2+} + H^+ \rightleftharpoons Fe^{3+}_{aq} + H_2L^{RA} \qquad k_1, k_{-1}\ K_1 \qquad (13)$$

$$\updownarrow K_h$$

$$Fe(HL^{RA})^{2+} \rightleftharpoons Fe(OH)^{2+}_{aq} + H_2L^{RA} \qquad k_1', k_{-1}', K_1' \qquad (14)$$

The shift of the absorbance maximum to longer wavelength is consistent with a bis complex dissociation to a mono complex.[22,25] The absorbance values at the end of the very fast absorbance drop and at the end of the first absorbance decay are related to reactions 11 and 12 through eqs 15 and 16 by assuming that a quasi equilibrium position is achieved whereby the next reaction does not proceed to a significant degree.

$$Abs_{eq}^1 = C_0 \frac{(\epsilon_{Fe(L^{RA})^+} + \epsilon_{Fe(HL^{RA})^{2+*}} K_5[H^+])}{1 + K_5[H^+]} \qquad (15)$$

$$Abs_{eq}^2 = C_0 \frac{(\epsilon_{Fe(L^{RA})^+} + \epsilon_{Fe(HL^{RA})^{2+*}} K_5[H^+] + \epsilon_{Fe(HL^{RA})^{2+}} K_6 K_5[H^+])}{1 + K_5[H^+] + K_6 K_5[H^+]} \qquad (16)$$

Abs_{eq}^1 and Abs_{eq}^2 are the absorbance at the quasi equilibrium position after reactions 11 and 12, respectively; C_0 represents the total $[Fe(L^{RA})^+]$; and $\epsilon_{Fe(L^{RA})^+}$, $\epsilon_{Fe(HL^{RA})^{2+*}}$, and $\epsilon_{Fe(HL^{RA})^{2+}}$ are the apparent molar extinction coefficients for the bis complex $Fe(L^{RA})$, the protonated intermediate $Fe(HL^{RA*})^{2+}$, and the mono hydroxamate iron(III) complex $Fe(HL^{RA})^{2+}$, respectively. The equilibrium absorbance data are presented in Figure 5 as a function of $[H^+]$. The total H^+ stoichiometry for reactions 11

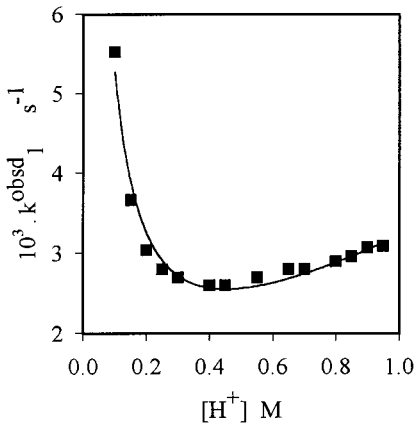

Figure 7. Variation of the observed dissociation rate constant k_1^{obsd} as a function of $[H^+]$ for $Fe(L^{RA})^+$ prepared in a 1:1 Fe:L ratio. Conditions: $[Fe^{3+}] = 0.1$ mM, $[L^{RA}] = 0.1$ mM, $I = 2.0$ M ($HClO_4$/$NaClO_4$), $T = 25$ °C, $[H^+] = 0.1-1.0$ M. The solid line represents a fit of the nonlinear eq 18 to the experimental data with the convergence parameters $a = 4.48 \times 10^{-4}$ (1.4×10^{-5}), $b = 5.7 \times 10^{-4}$ (5.5×10^{-5}), $c = 9.2 \times 10^{-4}$ (6×10^{-5}). Values in parentheses represent the standard error.

and 12, and the equilibrium constant for reaction 11 ($K_5 = 1.31$ M^{-1}), were determined from eqs 15 and 16. Equation 16 is too parameter intensive to be used to determine a value for the equilibrium constant for reaction 12.

The two absorbance decays monitored were well separated, and the apparent dissociation rate constants related to reactions 12, 13, and 14 were determined from a nonlinear monoexponential fit of the absorbance decay data over the time frame up to 2 s, and up to 1400 s (Figure 4). The apparent dissociation rate constant associated with reaction 12 shows a saturation profile with increasing $[H^+]$ (Figure 6) in agreement with the pre-equilibrium reaction 11 shown in Scheme 3. The apparent dissociation rate constant k_6^{obsd} is related to the parameters in reactions 11 and 12 by eq 17. Figure 6 contains the experimental

$$k_6^{obsd} = \frac{k_6 K_5 [H^+]}{1 + K_5 [H^+]} + k_{-6} \qquad (17)$$

data and the computed fit according to eq 17. Values for $k_6 = 7.98$ s^{-1}, $k_{-6} = 0.7$ s^{-1} and $K_5 = 1.25$ M^{-1} were determined in this manner. The value of K_5 determined from our kinetic results ($K_5 = 1.25$ M^{-1}) is in good agreement with the corresponding value obtained from the absorbance change at the quasi equilibrium positions ($K_5 = 1.31$ M^{-1}; Figure 5).

(C) Ligand Dissociation Kinetics of the Mono Complex. The slow final absorbance decay is associated with ligand dissociation from $Fe(HL^{RA})^{2+}$ by parallel paths according to reactions 13 and 14. The apparent dissociation rate constant related to this slow step shows inverse H^+ dependence at low $[H^+]$, followed by linear H^+ dependence at higher $[H^+]$ (Figure 7). This result is associated with parallel pathways involving reversible H^+ dependent and H^+ independent reactions 13 and 14. By assuming relaxation conditions, the rate law for reactions 13 and 14 is described by eq 18,[27]

$$k_1^{obsd} = a + \frac{b}{[H^+]} + c[H^+] \qquad (18)$$

where $a = k'_1$, $b = k'_{-1} K_h ([Fe^{3+}]_{tot} - [Fe(HL^{RA})^{2+}]_{eq})$, $c = k_1$. The solid line in Figure 7 represents a fit of eq 18 to the experimental data. The values of the rate constants $k_1 = 9.2 \times 10^{-4}$ M^{-1} s^{-1} and $k'_1 = 4.48 \times 10^{-4}$ s^{-1} were obtained. These results are consistent with the data in the literature for mono-hydroxamato Fe(III) ligand dissociation kinetics.[25-27]

Ligand Dissociation Kinetics for the Alcaligin−Iron(III) Complex. (A) Ligand Dissociation Kinetics of the Tris Complex. The tris complex of alcaligin−iron(III) ($Fe_2(L^{AG})_3$, $Fe(L^{AG})(HL^{AG})$) was prepared in a 2:3 Fe:L^{AG} ratio at neutral pH and 2.0 M ionic strength ($NaClO_4$/$HClO_4$). The ligand dissociation reaction was monitored at 425 nm by rapid mixing of equal volumes of the complex with an acid solution of desired concentration. The $[H^+]$ range was 0.001−0.07 M at 25 °C and constant ionic strength, $I = 2.0$ M ($NaClO_4$/$HClO_4$). Absorbance decays recorded on the time scale of 1−20 s, depending on the $[H^+]$, show monoexponential behavior (Figure 1D). Spectral changes recorded during this step (Figure 2B, spectra 1 and 2) show isosbestic behavior consistent with a tris to bis hydroxamato−iron(III) conversion.

A mechanism for the tris complex ligand dissociation that includes both a mono- and a diiron complex is shown in reactions 19 and 20. In considering the kinetics of ligand

$$Fe(L^{AG})(HL^{AG}) + H^+ \rightleftharpoons Fe(L^{AG})^+ + H_2L^{AG} \qquad k'_{10}, k'_{-10}K_{10} \quad (19)$$

$$Fe_2(L^{AG})_3 + H^+ \rightleftharpoons Fe(L^{AG})^+ + Fe(L^{AG})(HL^{AG}) \qquad k''_{10}, k''_{-10}K''_{10} \quad (20)$$

dissociation from the tris complex as $Fe(L^{AG})(HL^{AG})$ and $Fe_2(L^{AG})_3$, yet involving a single process, it is significant that a variation in the Fe:L^{AG} ratio up to 1:5 did not affect the monoexponential decay observed (Figure 1D). Also, our independent investigation by ESI-MS shows that the major tris complex present under conditions of excess ligand is the mono-Fe species $Fe(L^{AG})(HL^{AG})$.[18] An interpretation of the ligand dissociation kinetic data is to consider that the mono- and diiron species dissociate at the same rate, as illustrated by eqs 19 and 20. This assumption is reasonable, since the two metal centers in the complex $Fe_2(L^{AG})_3$ are noninteractive and protonation on either side should not affect the protonation on the second Fe center. The global reaction will be observed as a dissociation reaction involving one proton. The H^+-driven ligand dissociation reaction 19−20 exhibits an absorbance decay at 425 nm (Figure 2D) which can be analyzed as a mono-exponential decay. Figure 8 shows a plot of the pseudo-first-order rate constant ($[H^+]$ in excess) obtained for reaction 19−20 plotted as a function of H^+. A linear fit of eq 21 to the data shown in Figure 8 gives $k'_{10} = 158$ M^{-1} s^{-1} and $k'_{-10} \approx 0$.

$$k'^{obsd}_{10} = k'_{10}[H^+] + k'_{-10}[H_2L^{AG}] \qquad (21)$$

(B) Ligand Dissociation Kinetics of the Bis Complex Fe(L^{AG})$^+$. The dissociation of $Fe(L^{AG})^+$ was monitored at 470 nm in the $[H^+]$ range 0.1−1.0 M, $I = 2.0$ M, and 25 °C. Ligand dissociation from the bis complex is very slow; the absorbance decay at 470 nm recorded on a time scale of 20 h (!) is shown in Figure 1E. The spectral change observed during the acid dissociation showed an absorbance decrease at all wavelengths (Figure 2B, spectra 2 and 3). The absorbance decay follows a double-exponential behavior with poor reproducibility. The initial absorbance of the complex is not recovered when the pH of the dissociated complex solution is increased to the range where the complex $Fe(L^{AG})^+$ is stable. These results suggest that $Fe(L^{AG})^+$ dissociation under these acidic conditions proceeds with ligand decomposition. We were not able to achieve a

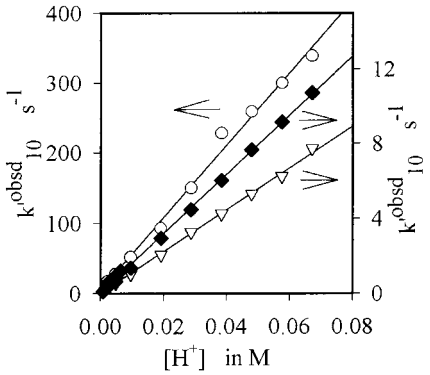

Figure 8. Plot of the observed dissociation rate constant k'^{obsd}_{10} as a function of $[H^+]$ for (◆) $Fe(L^{AG})(HL^{AG})$, (▽) $Fe(L^{AG})$(NMAHA), and (○) $Fe(L^{AG})$(glyHA). Values are presented on two different scales as shown by the arrows. The total complex concentrations were 0.2 mM at $I = 2.0$ M ($HClO_4/NaClO_4$), $T = 25$ °C. Solid lines represent fits of the following linear equation to the data: $k'^{obsd}_{10} = a[H^+] + c$; see eq 21. (○) $a = 5160$ (176), $b = 4.68(4)$; (◆) $a = 158$ (1.4), $b = 0.036$ (0.04); (▽) $a = 111$ (1.8), $b = -0.03$ (0.006). Values in parentheses represent the standard error.

complete analysis of the dissociation kinetics of the $Fe(L^{AG})^+$ complex. However, an average value for the apparent dissociation rate constant obtained in moderate acid concentration (0.1−0.3 M) was calculated by fitting the total absorbance decay according to a double-exponential equation (eq 3) where only the first constant is considered by assuming that the second decay is a result of ligand decomposition. The average value of the apparent dissociation constant in the $[H^+]$ range of 0.1−0.3 M is $k = 1 \times 10^{-5}$ M^{-1} s^{-1}. The dissociation rate of $Fe(L^{AG})^+$ (reactions 22−24, Scheme 4)

Scheme 4

$$Fe(L^{AG})^+ + H^+ \rightleftharpoons Fe(HL^{AG})^{2+} \qquad K_5 \qquad (22)$$

$$Fe(HL^{AG})^{2+} + H^+ \rightleftharpoons Fe^{3+}_{aq} + H_2L^{AG} \qquad k_1, k_{-1}\ K_1 \qquad (23)$$

$$\Updownarrow K_h$$

$$Fe(HL^{AG})^{2+} \rightleftharpoons Fe(OH)^{2+}_{aq} + H_2L^{AG} \qquad k_1', k_{-1}', K_1' \qquad (24)$$

based on this observation is ca. 10^4 times slower than the values observed for the synthetic linear chain dihydroxamic acid bis hydroxamato−iron(III) complex dissociation ($k_6 = 16$ M^{-1} s^{-1}).[22] This enhanced bis complex kinetic stability is attributed to the rigidity and preorganization of the alcaligin ligand. This effect results in a small dissociation equilibrium constant, K_5, as a result of enhanced back reaction kinetics; i.e., a large k_{-5}.

(C) Ligand Dissociation Kinetics of the Ternary Complexes $Fe(L^{AG})(L)$. Ternary complexes may be readily prepared in situ by adding a stoichiometric amount of a synthetic monohydroxamic acid (HL, *N*-methylacetohydroxamic acid, NMAHA, or glycine hydroxamic acid, glyHA) to an aqueous solution of $Fe(L^{AG})^+$ to produce $Fe(L^{AG})(L)$. The two complexes prepared in this way give spectra characteristic of a tris hydroxamato iron(III) complex with $\lambda_{max} = 425$ nm and $\epsilon = 2800-2500$ M^{-1} cm^{-1}. The dissociation kinetics of the glycine hydroxamic acid−alcaligin ternary complex is of interest for the purpose of studying the effect of the positive charge on the tris hydroxamato complex dissociation mechanism as a model for the ferrioxamine B siderophore (Figure 9). The tris complex with *N*-methylacetohydroxamic acid also provides a good model for comparison with $Fe(L^{AG})(HL^{AG})$ (Figure 9). It is also of interest to study the effect of alcaligin preorganization[15−17] in $Fe(L^{AG})^+$ for stabilizing the tris complexes. A kinetic investigation of the dissociation of *N*-methylacetohydroxamic acid from $Fe(L^{AG})$(NMAHA) (Figure 9) is a good model to support our assignment of the tris alcaligin complex dissociation to the species $Fe(L^{AG})(HL^{AG})$.

Ligand dissociation from the ternary complexes $Fe(L^{AG})(L)$ was studied at the same $[H^+]$ concentrations as the tris alcaligin−Fe(III) complex and monitored at 425 nm. Absorbance decay data as a function of time recorded during ligand dissociation from the ternary complexes $Fe(L^{AG})$(NMAHA) and $Fe(L^{AG})$(glyHA) are shown in Figure 10. The $Fe(L^{AG})$(NMAHA) complex shows the same behavior as the alcaligin complex prepared in a 2:3 Fe:L^{AG} ratio. The absorbance decay is monoexponential, and no absorbance variation is observed on a longer time scale (up to 200 s) at the H^+ concentration investigated ($[H^+] = 0.001-0.07$ M; Figure 10A). The apparent ligand dissociation rate, determined by fitting the absorbance decay signal by a mono-exponential function, is first-order with respect to $[H^+]$ (Figure 8). The corresponding dissociation reaction is described in eq 25, and the second-order dissociation rate constant ($k'_{10} = 111$ M^{-1} s^{-1}; $k_{-10} \approx 0$) was determined by a fit of eq 21 to the data (Figure 8).

$$Fe(L^{AG})(NMAHA) + H^+ \rightleftharpoons Fe(L^{AG})^+ + HNMAHA \qquad k'_{10}, k'_{-10} \qquad (25)$$

The ligand dissociation behavior of the tris complex $Fe(L^{AG})$-$(glyHA)^+$ is more complex; multistep behavior is observed as shown in Figure 10B. Time dependent spectra recorded using a diode array spectrophotometer are shown in Figure 11A for a 1 s time scale and Figure 11B for a 20 s time scale. Spectra in Figure 11A exhibit an isosbestic point at 470 nm. This behavior is characteristic of tris hydroxamato−iron(III) conversion to a bis hydroxamato−iron(III) complex. Spectra in Figure 11B do not show displacement of the absorbance maximum over 470 nm and result in a global absorbance decay. In the $[H^+]$ range used (0.001−0.05 M), alcaligin ligand decomposition is not observed. At a fixed wavelength ($\lambda = 425$ nm) the ligand dissociation proceeds by a fast monoexponential absorbance decrease, followed by a double-exponential absorbance decay (Figure 10B). Scheme 5 is consistent with our kinetic results for ternary complex ligand dissociation, where the glycine hydroxamic acid ligand completes the coordination of the bis alcaligin complex using two distinct binding modes, I and II, in Figure 9. Reaction 26 involves $Fe(L^{AG})(glyHA)^+$ in coordination mode I and reactions 27 and 28 in coordination mode II.

Scheme 5

$$Fe(L^{AG})(glyHA_I)^+ + H^+ \rightleftharpoons Fe(L^{AG})^+ + HglyHA^+ \qquad k'_{10}, k'_{-10}, K'_{10} \qquad (26)$$

$$Fe(L^{AG})(glyHA_{II})^+ + H^+ \rightleftharpoons Fe(L^{AG})(HglyHA_{II})^{2+} \qquad k_{11}, k_{-11}, K_{11} \qquad (27)$$

$$Fe(L^{AG})(HglyHA_{II})^{2+} \rightleftharpoons Fe(L^{AG})^+ + HglyHA^+ \qquad k_{12}, k_{-12}, K_{12} \qquad (28)$$

The ternary tris hydroxamate complex I dissociates in one step according to reaction 26. The apparent dissociation rate constant related to the dissociation reaction is determined by fitting the first absorbance decay by a monoexponential equation. First-order dependence on $[H^+]$ is observed (Figure 8). The apparent dissociation rate is related to the proton concentration through eq 29; the rate constant $k'_{10} = 5160$ M^{-1} s^{-1} was determined from a linear fit of eq 29 to the experimental data in Figure 8.

$$k'^{obsd}_{10} = k'_{10}[H^+] + k'_{-10}[HglyHA] \qquad (29)$$

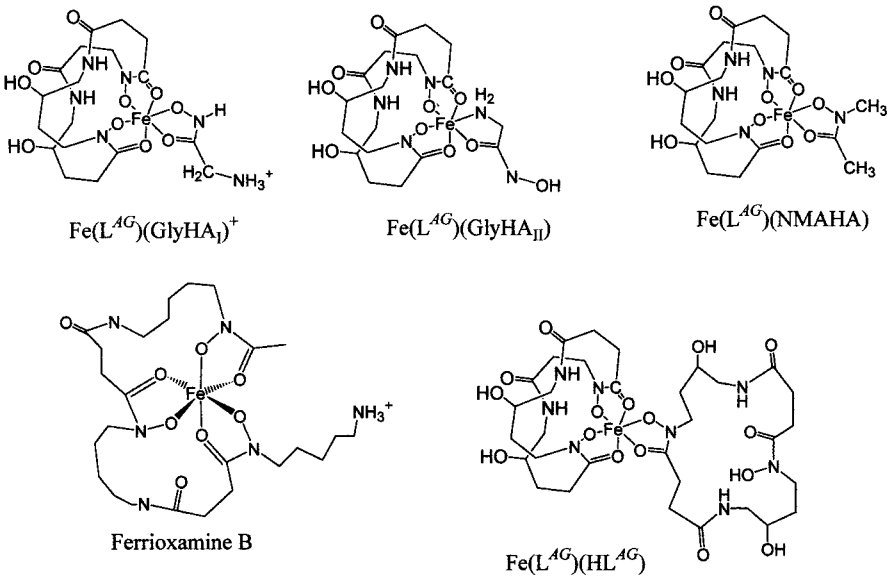

Figure 9. Proposed structures for the tris Fe(III) complex of alcaligin, ternary alcaligin/glycine hydroxamic acid complexes with different bonding modes I and II, ternary alcaligin/*N*-methylacetohydroxamic acid complex, and ferrioxamine B.

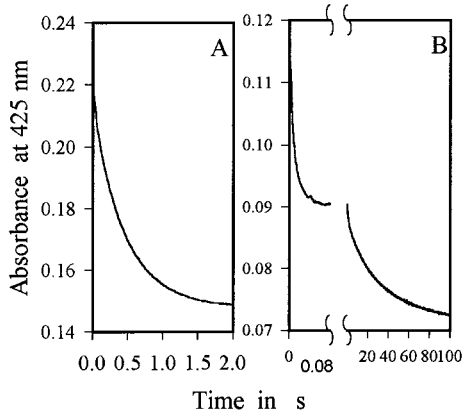

Figure 10. Absorbance decay (λ = 425 nm; optical path 1 cm) recorded during the H^+-driven ligand dissociation of the alcaligin ternary complexes with NMAHA (Fe(L^{AG})(NMAHA)) (A) and glycine hydroxamic acid (Fe(L^{AG})(glyHA)) (B). Reactions initiated by a [H^+] jump from $10^{-6.5}$ to 0.02 M. Conditions: [H^+] 0.02 M, I = 2.0 M($HClO_4$/$NaClO_4$), T = 25 °C. (A): [Fe^{3+}] = 0.1 mM, [H_2L^{AG}] = 0.1 mM, [NMAHA] = 0.1 mM. (B): [Fe^{3+}] = 0.05 mM, [H_2L^{AG}] = 0.05 mM, [glyHA] = 0.05 mM.

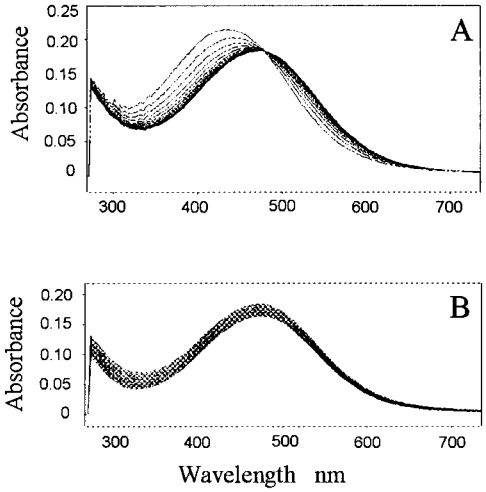

Figure 11. Time dependent spectra recorded over a 1 s (A) and 20 s (B) time scale during the H^+-driven ligand dissociation from the ternary alcaligin−glycine hydroxamic acid complex Fe(L^{AG})(glyHA). Conditions: [H^+] = 0.003 M, optical path 1 cm, I = 2.0 M ($HClO_4$/$NaClO_4$), [Fe^{3+}] = 0.1 mM, [H_2L^{AG}] = 0.1 mM, [glyHA] = 0.1 mM.

The second and third steps observed in the ligand dissociation from Fe(L^{AG})(glyHA)$^+$ are attributed to the dissociation of the tris complex Fe(L^{AG})($glyHA_{II}$)$^+$ according to eqs 27 and 28. The first step is attributed to protonation of the coordinated amine nitrogen group followed by proton independent dissociation of the complex in the next step. The apparent dissociation constants for reactions 27 and 28 were determined from numerical fitting of the absorbance decay by a double-exponential equation (eq 3). A plot of k_{11} and k_{12} with respect to H^+ shows first-order dependence of k_{11} and a saturation profile for k_{12} (Figure 12). The apparent dissociation rate constants k_{11}^{obsd} and k_{12}^{obsd} are associated with the microscopic rate constants for reactions 27 and 28 through eqs 30 and 31.

$$k_{11}^{obsd} = k_{11}[H^+] + k_{-11} \quad (30)$$

$$k_{12}^{obsd} = \frac{k_{12}K_{11}[H^+]}{1 + K_{11}[H^+]} + k_{-12}[HglyHA] \quad (31)$$

A fit of eq 30 to the data yields k_{11} = 32.9 M^{-1} s^{-1} and k_{-11} = 0.16 s^{-1}, and a fit of eq 31 yields k_{12} = 0.024 s^{-1}, and K_{11} = 186 M^{-1} (Figure 12). The value of K_{11} (186 M^{-1}) from eq 31 is in good agreement with the value computed as k_{11}/k_{-11} (205 M^{-1}).

Values for the microscopic rate and equilibrium constants for individual steps in the ligand dissociation reactions of the Fe(III) complexes of rhodotorulic acid and alcaligin, and ternary complexes involving *N*-methylacetohydroxamic acid and glycine hydroxamic acid, are listed in Table 1.

Discussion

Alcaligin Complexes. The recent X-ray crystal structure of the alcaligin−iron(III) complex isolated from a solution containing Fe:L^{AG} in a 2:3 ratio shows a singly bridged species (L^{AG})-Fe(L^{AG})Fe(L^{AG}).[16] Recent investigation of the alcaligin−iron(III) complex system by ESI-MS at variable Fe:L^{AG} ratios showed the presence of the mono-Fe complex Fe(L^{AG})(HL^{AG}) in addition to $Fe_2(L^{AG})_3$.[18] From our current investigation, we did not

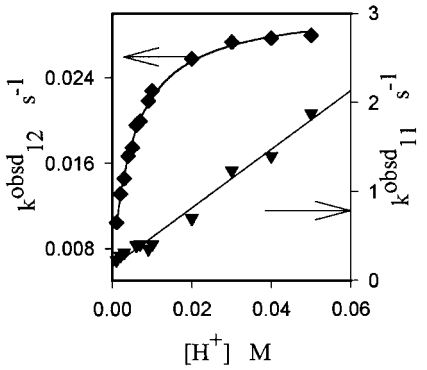

Figure 12. Variation of the observed dissociation rate constants for the second (eq 27; k_{11}^{obsd}; ▼) and third (eq 28; k_{12}^{obsd}; ◆) steps in the dissociation of the ternary complex Fe(L^{AG})(glyHA) as a function of [H^+]. Conditions: $I = 2.0$ M ($HClO_4$/$NaClO_4$), [Fe^{3+}] = 0.1 mM, [L^{AG}] = 0.1 mM, [glyHA] = 0.1 mM, $T = 25$ °C. Values are presented on two different scales as shown by the arrows. Solid lines represent fits of the linear eq 30 (▼) $k_{11}^{obsd} = a[H^+] + b$, $a = 32.9$ (1.5), $b = 0.16$ (0.2), and nonlinear eq 31 (◆) $k_{12}^{obsd} = a[H^+]/(1 + b[H^+]) + c$, $a = 5.53$ (0.46), $b = 186$ (16.5), $c = 0.006$ (6×10^{-4}), to the data. Values in parentheses represent the standard error.

Table 1. Kinetic Parameters for Proton-Driven Dissociation Reaction of Tris, Bis, and Mono Iron(III) Complexes of Rhodotorulic Acid and Alcaligin, and Ternary Complexes Containing Alcaligin

ligand dissociation	reaction no.	parameter	value[a]
	Rhodotorulic Acid Complexes		
tris → bis	4 and 5	$K_{11}k_{10}/M^{-1}\,s^{-1}$	678
	4′ and 6	$K'_{11}k'_{10}/M^{-1}\,s^{-1}$	3839
bis → mono	9	$k_7/M^{-1}\,s^{-1}$	69
	11	K_5/M^{-1}	1.31[b] (1.25)[c]
	12	K_6	11.4[d]
	12	k_6/s^{-1}	7.98
	12	k_{-6}/s^{-1}	0.7
mono → aquo	13	$k_1/M^{-1}\,s^{-1}$	9.2×10^{-4}
	14	k'_1/s^{-1}	4.48×10^{-4}
	Alcaligin Complexes		
tris → bis	19/20	$k'_{10}/M^{-1}\,s^{-1}$	158
bis → aquo	22−24	$K_5k'_1/M^{-1}\,s^{-1}$	1×10^{-5}
	Ternary Alcaligin Complexes		
tris → bis			
NMAHA dissociation	25	$k'_{10}/M^{-1}\,s^{-1}$	111
glyHA dissociation	26	$k'_{10}/M^{-1}\,s^{-1}$	5160
	27	$k_{11}/M^{-1}\,s^{-1}$	32.9
	27	k_{-11}/s^{-1}	0.16
	27	K_{11}/M^{-1}	186[e] (205)[f]
	28	k_{12}/s^{-1}	0.024

[a] Uncertainties are defined in figure captions. [b] Value obtained from absorbance change at the quasi equilibrium position; Figure 5. [c] Value obtained from kinetic results according to eq 17 and Figure 6. [d] Value calculated from $K_6 = k_6/k_{-6}$. [e] Value obtained from kinetic results. [f] Value calculated from the ratio k_{11}/k_{-11}.

observe any difference in the dissociation kinetics obtained at a 2:3 Fe:L^{AG} ratio and those obtained in the presence of excess ligand (up to Fe:L^{AG} = 1:5). We attribute the observed kinetics to the dissociation of Fe(L^{AG})(HL^{AG}) according to eq 19 with a rate constant $k'_{10} = 158$ $M^{-1}\,s^{-1}$. This assignment is supported by the ligand dissociation kinetics of the ternary complex Fe(L^{AG})(NMAHA) according to eq 25 with a second-order rate constant $k'_{10} = 111$ $M^{-1}\,s^{-1}$, as well as the dissociation of NMAHA from Fe(L^8)(NMAHA) ($H_2L^8 = H_3CN(OH)C(=O)-(CH_2)_8(C=O)N(OH)CH_3$; $k = 316$ $M^{-1}\,s^{-1}$).[22] These kinetic results are also consistent with the presence of the tris complex (L^{AG})Fe(L^{AG})Fe(L^{AG}) where the two Fe centers are noninteractive and equivalent, and consequently the dissociation kinetics are the same as for the mono-Fe species Fe(L^{AG})(HL^{AG}) (Figure 9).

A structural representation of the overall ligand dissociation scheme for the alcalgin−Fe(III) system is shown in Scheme 6. The dissociation of the tris complex of alcaligin proceeds in a single path, and the only bis complex resulting from ligand dissociation from Fe(L^{AG})(HL^{AG}) is Fe(L^{AG})$^+$. This is undoubtedly due to the high level of preorganization of the alcaligin ligand and the enhanced stability of the Fe(L^{AG})$^+$ species.[15,16] Due to the cyclic structure of the preorganized alcaligin ligand, in the protonated species the protonated group remains close to the metal center. As was previously discussed, the limiting step in the iron(III)−hydroxamate complex dissociation is governed by the displacement of the carbonyl group.[27] By maintaining the dissociated site in close proximity to the metal as a result of this structural rigidity, the recombination reaction is enhanced, leading to an extremely stable complex. Under our conditions the dissociation of the tris complex should proceed unambiguously through the species Fe(L^{AG})$^+$, as illustrated in the proposed mechanism (Scheme 6). The ligand dissociation rate constant for the ternary complex Fe(L^{AG})(NMAHA) ($k'_{10} = 111$ $M^{-1}\,s^{-1}$) is in good agreement with this interpretation.

The dissociation kinetics of the ternary complex with glycine hydroxamic acid, Fe(L^{AG})(glyHA)$^+$, were investigated in part as a model for ferrioxamine B. The free side chain for bonding mode I (Fe(L^{AG})($glyHA_I$)$^+$; Figure 9) has a positive charge and represents a good mimic to examine whether or not a positive charge has any effect on ligand dissociation from the complex. The two distinct ligand dissociation reactions observed for the glycine hydroxamic acid ternary complex are attributed to two complexes of different glycine hydroxamic acid binding modes (I and II: Figure 9). The tris hydroxamate binding mode (I) dissociates in the presence of an increasing [H^+] in one step leading to a first-order proton dependent reaction (eq 26) with a rate constant $k'_{10} = 5161$ $M^{-1}\,s^{-1}$. The tris → bis dissociaton kinetics are more rapid for Fe(L^{AG})($glyHA_I$)$^+$ than for Fe(L^{AG})-(NMAHA) due to the previously documented reduced dissociation lability for N−CH_3 relative to N−H hydroxamate ligands.[22,27] However, comparison of Fe(L^{AG})($glyHA_I$)$^+$ dissociation kinetics with other N−H hydroxamate ligand dissociation reactions shows that the positive charge on the side chain has a negligible effect on the dissociation rate. The kinetics of acetohydroxamic acid (AHA) dissociation from a ternary complex is illustrated in reaction 32, where L^8 is a synthetic dihydroxamate ligand

$$\mathrm{Fe}(L^8)(\mathrm{AHA}) + H^+ \rightleftharpoons \mathrm{Fe}(L^8)^+ + \mathrm{HAHA} \qquad K'_{10}, k'_{10}, k'_{-10} \quad (32)$$

with an eight-carbon chain between hydroxamate groups ($\{CH_3N(O^-)C(O)\}_2(CH_2)_8$; $(L^8)^{2-}$) and AHA is the acetohydroxamate anion ($CH_3C(O)N(O^-)H$). The rate constant for reaction 32 is $k'_{10} = 4.5 \times 10^3$ $M^{-1}\,s^{-1}$.[22] This is also consistent with primary (N−H) hydroxamic acid dissociation from other uncharged tris hydroxamate−iron(III) complexes.[25,33] The second reaction arising from the other glycine hydroxamic acid coordination mode II (Figure 9) shows a saturation profile with respect to [H^+] and is attributed to two successive reactions (eqs 27 and 28), where the first reaction is H^+ dependent arising from protonation and ring opening, followed by a second H^+ independent step due to ligand dissociation from the complex.

(33) Biruš, M.; Bradic, Z.; Kijundzic, N.; Pribanic, M.; Wilkins, R. G. *Inorg. Chem.* **1985**, *24*, 3980.

Scheme 6. Ligand Dissociation Mechanism for the Fe(III) Alcaligin Complexes[a]

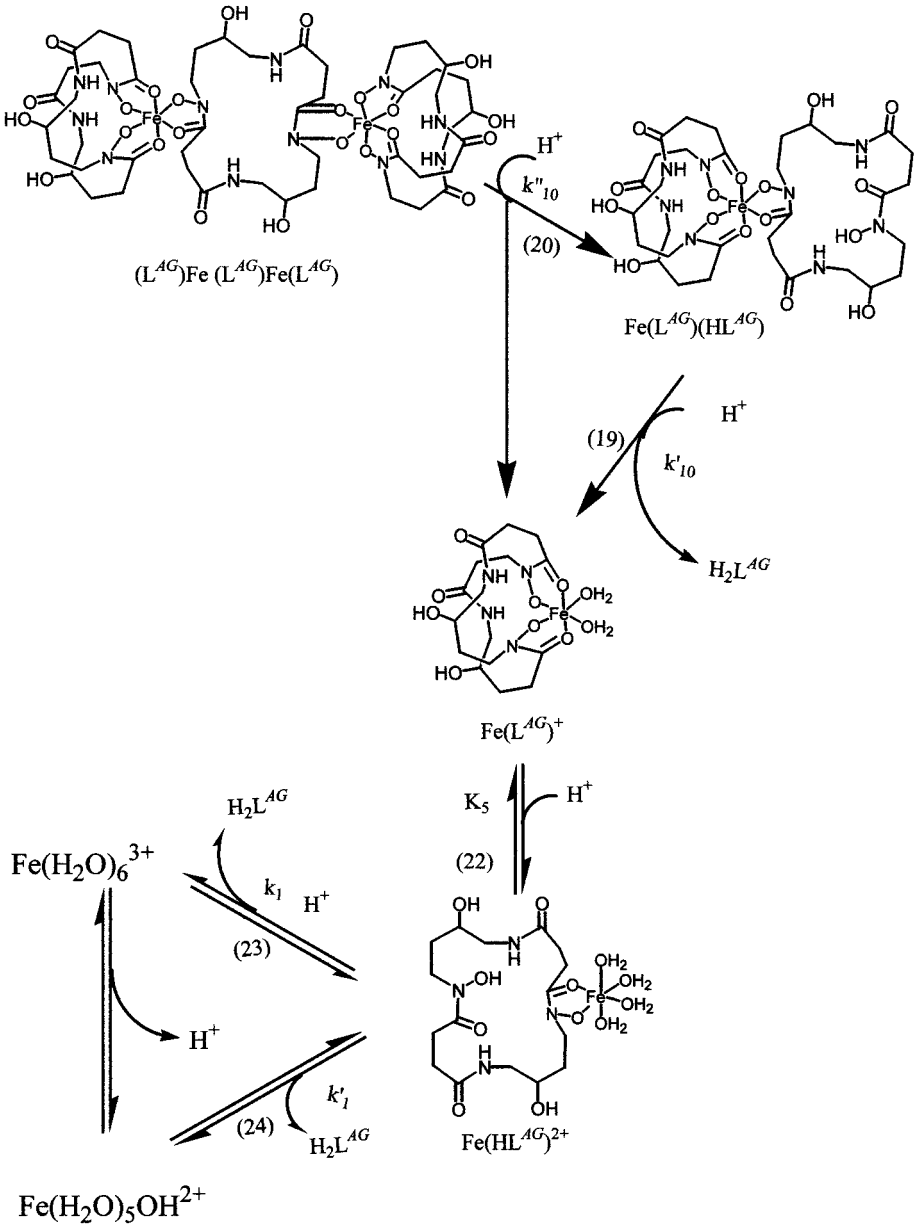

[a] Numbers in parentheses correspond to reaction numbers in the text.

The bis complex of the alcaligin−iron(III) system, $Fe(L^{AG})^+$, is stable over a wide range of $[H^+]$ as a result of ligand rigidity and preorganization, as was discussed in the previous section. Only partial dissociation of $Fe(L^{AG})^+$ is observed, even at high $[H^+]$ where the ligand undergoes slow decomposition. The dissociation rate determined from considering the average values of the experiment carried out at moderate $[H^+]$ yields a dissociation rate constant $k = K_5k'_1 = 1 \times 10^{-5}$ M^{-1} s^{-1}. This value is out of the range observed for bis complex dissociation and reflects the extreme stability of the $Fe(L^{AG})^+$ complex (Scheme 6).

Rhodotorulic Acid Complexes. Previous thermodynamic investigations[6] of the iron(III)−rhodotorulic acid system were interpreted in terms of the formation of $Fe_2(L^{RA})_3$, which was assumed to exhibit a triply bridged structure, based on an X-ray crystal structure of a model synthetic complex.[19] In our ESI-MS investigation of the structure of the rhodotorulic acid complexes, solutions prepared in a 2:3 Fe:L^{RA} ratio and in excess ligand displayed mainly the monometallic species $Fe(L^{RA})(HL^{RA})$.[18] For solutions prepared in a 1:1 Fe:L^{RA} ratio, the main structure was the monometallic species $Fe(L^{RA})^+$.[18] In the present kinetic investigation of the rhodotorulic acid complex in a 1:1 Fe:L^{RA} ratio, our results support the ESI-MS investigation and confirm the stoichiometry of the bis complex as $Fe(L^{RA})^+$ (as opposed to $Fe(L^{RA})_2Fe^{2+}$). Based on our previous kinetic investigation of a number of Fe(III) complexes with linear synthetic dihydroxamic acid ligands ($\{CH_3N(OH)C(O)\}_2\{CH_2\}_n$, L^nH_2 where $n = 2-8$), the dissociation kinetics of a doubly ligand bridged species ($(H_2O)_2Fe(L^n)_2Fe(H_2O)_2^{2+}$) exhibits second-order H^+ dependence with a strong rate dependence on the Fe−Fe distance.[22,26] The dissociation of the rhodotorulic acid−iron(III) complex prepared in a 1:1 Fe:L^{RA} ratio shows overall first-order dependence on $[H^+]$, consistent with a mono-Fe structure, $Fe(L^{RA})^+$. This result is similar to the dissociation kinetics of the synthetic linear analogues adopting a mono-Fe binding mode, $Fe(L^n)^+$.[22,26] Under the conditions of a 2:3 Fe:L^{RA} ratio the dissociation kinetics are again inconsistent with a ligand-bridged structure, since no

Scheme 7. Ligand Dissociation Mechanism for the Fe(III) Rhodotorulic Acid Complexes[a]

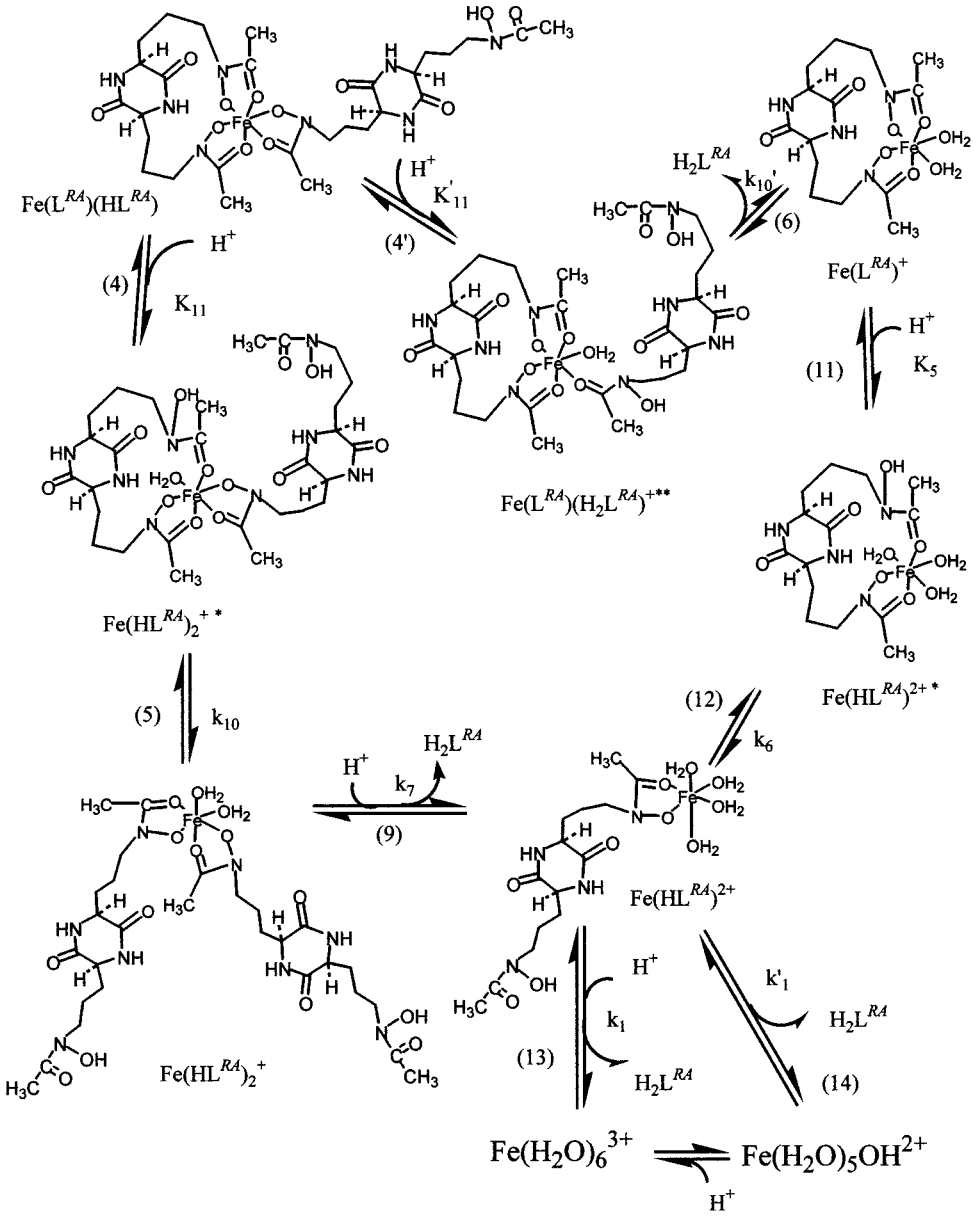

[a] Numbers in parentheses correspond to reaction numbers in the text.

second-order dependence on $[H^+]$ concentration was observed, as we would expect from comparison with the dissociation kinetics of the linear analogues adopting a triply bridged di-Fe structure.[22] Ligand dissociation kinetics results for the tris complex of rhodotorulic acid−iron(III) are consistent with the stoichiometry $Fe(L^{RA})(HL^{RA})$, which is supported by our ESI-MS results.[18]

A structural representation of the overall ligand dissociation scheme for the rhodotorulic acid−Fe(III) system is shown in Scheme 7. The complex $Fe(L^{RA})(HL^{RA})$ (Scheme 2) adopts a monometallic tris hydroxamate binding mode with three equivalent hydroxamate units. As the pH is lowered to the condition where the bis complex is more stable, the tris complex dissociates to the bis complex. The first protonation can occur with equal probability on any of the three hydroxamate units binding the Fe(III) center, as illustrated in Scheme 2. Rapid protonation of the complex on sites A or B lead to the same intermediate, $Fe(HL^{RA})_2{}^{+}*$, that dissociates in a H^+ independent step to the bis complex, $Fe(HL^{RA})^{+}{}_2$. When protonation occurs on site C, the tris complex undergoes H_2L^{RA} ligand dissociaton to the bis complex, $Fe(L^{RA})^+$. The dissociation rate is apparently affected by the structure of the intermediate species, with ring opening via reactions 4 and 5 proceeding at a slower rate than ligand dissociation via reactions 4′ and 6 (Table 1). In both cases the overall reaction result is a tris to bis complex conversion. The reason for the rate constant difference may be due to the hydrophobic barrier afforded the entering H^+ at sites A and B (Scheme 2) by the closed dihydroxamate ring. The same effect is observed for "half-coordinated" synthetic linear dihydroxamic acid complexes of Fe(III), where complexes of the structure $Fe(HL^n)_2$ ($k_{10} = 65\ M^{-1}\ s^{-1}$) dissociate with much higher rates compared to complexes adopting a closed-ring structure, Fe-(L^n) ($k_{10} = 0.38\ M^{-1}\ s^{-1}$) ($H_2L^n$ represents the synthetic tetradentate dihydroxamate ligand $H_3CN(OH)C(=O)(CH_2)_n$-$C(=O)N(OH)CH_3$, $n = 2-8$).[22] This is observed in the extreme case for the alcaligin system where protonation and dissociation of the hydroxamate group from the tetracoordinated alcaligin ring of the tris complex $Fe(L^{AG})(HL^{AG})$ is not even observed (Scheme 6).

The ligand dissociation reaction from the bis complex of Fe-

(III)−rhodotorulic acid ($Fe(L^{RA})^+$ and $Fe(HL^{RA})_2^{+}$) was investigated under two sets of conditions. In one, the bis complex was prepared in a 1:1 Fe:L^{RA} ratio and, according to our independent ESI-MS analysis,[18] has the mono-Fe structure $Fe(L^{RA})^+$. Kinetic data under 1:1 Fe:L^{RA} conditions support the existence of $Fe(L^{RA})^+$ with no evidence for the species $Fe(HL^{RA})_2^{+}$. Under the other set of conditions, starting from the fully coordinated tris complex at a 2:3 Fe:L^{RA} ratio, a dissociation step attributed to the species $Fe(HL^{RA})_2^{+}$ is observed. These results support the dual path dissociation proposed for the tris rhodotorulic acid complex (Scheme 7). The dissociation scheme for the bis complex incorporates both structures ($Fe(HL^{RA})_2^{+}$ and $Fe(L^{RA})^+$); however, only the path associated with the $Fe(L^{RA})^+$ species is operative when starting from the complex prepared in a 1:1 Fe:L^{RA} ratio.

The first protonation step at $Fe(L^{RA})^+$ is fast, leading to an intermediate species that undergoes decomposition in two steps. The second step in the dissociation of the complex $Fe(L^{RA})^+$ (reaction 12) is a H^+ independent reaction which dissociates with a larger rate constant, $k_6 = 7.9\ s^{-1}$, than for synthetic analogues.[22,26] The corresponding reaction for ligand dissociation from $Fe(L^n)$ with synthetic linear dihydroxamate complexes of similar structure yields the rate constants $k_6 = 0.13\ s^{-1}$ (H_2L^8) and $k_6 = 0.38\ s^{-1}$ (H_2L^7)[26] where n is the carbon chain length between the two hydroxamate units. The increase in the dissociation rate constant k_6 may be due to higher strain in the chelation ring for $Fe(L^{RA})^+$ compared to the linear dihydroxamate ligand $Fe(L^8)^+$ and $Fe(L^7)^+$.

The slow step observed in the $[H^+]$ range of 0.1−1.0 M for the rhodoturolic acid complex is a common dissociation step observed for monohydroxamate complexes. The process is composed of parallel paths involving hexaaqua iron, $Fe(H_2O)_6^{3+}$, and the monohydroxo species $Fe(H_2O)_5(OH)^{2+}$, according to a relaxation mechanism as discussed previously.[25−27]

Conclusions

The influence of a high level of ligand preorganization for alcaligin, on one hand, and no level of preorganization for rhodotorulic acid, on the other hand, clearly influences the available ligand dissociation paths and intermediates, as well as reactivities, for the Fe(III) complexes of these two bacterial Fe carriers. In contrast to the hexadentate siderophores, the tetradentate siderophores as illustrated here by alcaligin and rhodotorulic acid, and elsewhere by synthetic models,[22] can undergo ligand dissociation by multiple paths providing intermediates of different structures, depending on environmental conditions (pH, Fe:L ratio). The existence of these multiple paths may facilitate cellular Fe release by catalytic processes (e.g., ternary complex formation) and may be justification for the biosynthesis of tetradentate siderophores, although their relative molar concentration must be higher than for hexadentate siderophores in order to coordinatively saturate the Fe.

The tris Fe(III) complexes of alcaligin and rhodotorulic acid both behave as though their Fe_2L_3 species adopt a monobridged structure, $(L^X)Fe(L^X)Fe(L^X)$ (X = RA, AG). This is consistent with the crystal structure for the alcaligin complex,[16] but in contrast with the sometimes-inferred triply bridged helicate structure for the rhodotorulic acid complex based on a X-ray crystal structure of a synthetic dihydroxamate complex, $Fe(L)_3Fe$.[19] We find no kinetic evidence for Fe−Fe interaction in these bimetallic siderophore complexes. This is consistent with an examination of the literature related to siderophore chemistry which reveals that, among the wide variety of complexes studied, none of them display a bimetallic structure with interacting metal centers. Interacting bimetallic centers may be expected to exhibit significant reactivity, as is demonstrated by the importance of diiron complexes in biological systems. Since the role of siderophore complexes is restricted in nature to Fe transport and storage, the biosynthetic design of these natural chelators is to prevent the formation of reactive diiron species. This fact should be considered in the design of synthetic siderophore mimics to prevent toxicity that can result from the formation of reactive oxygen species catalyzed by diiron species, for example.

Acknowledgment. We thank the NSF for financial support.

IC000330K